Fabrication of Asymmetric Polysaccharide Composite Membranes as Guided Bone Regeneration Materials

Na Li[1], Mingyan Zhao[2], Bihua Ye[1], Lihua Li[1,3,*], Lu Lu[1,3], Shan Ding[1,3], Changren Zhou[1,3,*], Hong Li[1,3], Yanpeng Jiao[1,3] and Mingxian Liu[1,3]

[1]*Department of Materials Science and Engineering, Jinan University, Guangzhou, 510632*

[2]*Stem Cell Research and Cellular Therapy Center, Affiliated Hospital of Guangdong Medical University, Zhanjiang, China*

[3]*Department of Stomatology of Medical College, Jinan University, Guangzhou 510632, China*

Abstract: Periodontal regeneration can be achieved by guided tissue and guided bone regeneration (GTR/GBR) membranes, which act as a physical barrier to exclude migration of connective and epithelium, favoring the repopulation of periodontal ligament cells. Asymmetric polysaccharide GBR membranes with two different surfaces were developed in this study. Positive chitosan (CS), negative hyluronaic acid (HA) and konjac glucomannan (KGM) were composited by electrostatic interaction, forming smooth and dense membranes as upper surface to inhibit the ingrowth of cells from gingiva. The lower porous and coarse surface was obtained by gel freeze-drying and mineralization to improve the regeneration of the bone tissue. The performance of the membranes was characterized by Infrared Radiation (IR), X-ray diffraction (XRD), scanning electron microscope (SEM), tensile strength and biological evaluation. It was found that the composite membranes with chitosan content of 56.7 wt%in the dry state possess the highest tensile strength, with elongation 10 times more higher than that of the pure CS ones. Additionaly, open pores with diameter of 10-100 μm and homogenouse distributed nano-hydroxyapatite (HAP) were investigated on the coarse part. Cell studies demonstrated that the porous surface promoted the growth of the preosteoblast. Overall, the composite membranes may be useful for regeneration of periodontal regeneration.

Keywords: Periodontal regeneration, Guided bone regeneration, Chitosan, Asymmetric membrane, Mineralization.

1. INTRODUCTION

Recent research has focused upon use of bone substitutes in combination with the GTR barriers for better clinical outcomes of periodontal regenerative procedures, which delays the apical migration of the gingival epithelium by excluding the gingival connective tissue and allows granulation tissue derived from the periodontal ligament and osseous tissues to repopulate the space adjacent to the denuded root surface through the use of barrier membranes [1, 2].

The bioabsorbable membranes are the second-generation GTR membranes and were developed to avoid the second surgical procedure to remove the barrier. These commercial GTR devices fall into two broad categories[3]: collagen membranes such as AlloDerm®, Periocol®, BIOgide®, and BioMend Extend®; and the synthetic (copolymers) materials like Guidor®, Cytoplast® , Vicryl periodontal mesh, Resolut Adapt® and the Atrisorb® GTR barrier. Except the above products, there are many other hot candidate materials used for basic and application research, for example , collagen films with different origin [2, 4, 5], amnion [6], electrospun biodegradable polyester membranes [7-9], or biohybrids [10, 11]. Collagen has been used extensively, but such materials are derived from animal sources and have an associated risk of disease transmission and associated ethical and cultural issues. Moreover, the fast resorption rate of this material and its poor mechanical strength are a concern to many clinicians [12]. Synthetic materials although have many more obvious advantages over collagen, such as tolerable mechanical strength and biodegradation, the relatively lower compatibility limit their application. Upon selecting an ideal biomaterial for GTR membranes, the following requirements must be considered: wound stabilization, space creation and maintenance, protection of the underlying blood clot, and the ability to exclude unwanted tissues or cells. Therefore natural and modified polysaccharide is arousing the interest of researchers.

Among the various natural polymers, chitosan (CS) has been regarded as one of the most suitable materials, owing to its biocompatibility, biodegradability, hemostaticity, and anti-bacterial effects [13-15]. Hyaluronic acid (HA) composite materials are the most extensively tested adhesion prevention agent in general surgery, such as Seprafilm®, which is safe and effective in reducing the migration of the epithelium and fibroblast [16-18]. However the mechanical strength of

*Address correspondence to this author at the Department of Stomatology of Medical College, Jinan University, Guangzhou 510632, China;
Tel: 0086-20-85226663; Fax: 0086-20-85223271;
E-mail: tlihuali@jnu.edu.cn; tcrz9@jnu.edu.cn

E-ISSN: 2409-3394/15

such biomaterials needs to be improved. Konjac glucomannan (KGM) is composed of D-glucose (G) and D-mannose (M) compound polysaccharide with the molar ratio of about 1: 1.6 linked by glycosidic bond. KGM possess stronger reactivity and good biodegradability. Several researches have proved that the degradation velocity of KGM membranes is 8-12 weeks [19, 20]. One of our previous studies found that the containing of KGM can improve the biodegradation of CS, and the toughness of the membranes [21].

With GTR/GBR approach, both wide/deep and narrow/shallow intrabony defects have been showed comparable almost complete regeneration of the periodontal attachment [2]. Membranes for GTR/GBR applications capable of promoting faster bone growth as well as impeding the infiltration of epithelial tissue into the defect and bacterial colonization would be unique and highly effective when implanted *in vivo*. Furthermore, space-providing porous GBR membranes have been demonstrated effective devices in support of periodontal wound healing/regeneration with limited postoperative complications compared with occlusive membranes [22]. An effective technique by using asymmetric membranes, has been widely used in the treatment of serious periodontal disease[23], with one side occluding cells from surrounding soft tissues and the other side providing spaces for the remodeling of alveolar bones. The porous side is often clinically combined with bone matrix such as bone ash, Bio-Oss® or nano-hydroxyapatite (HAP). However, there are still some points needed to be improved, including tissue integration, the suppressing of bacterial, and the transport of body fluids.

Coupled with its osteoconductivity and osteoinductivity, HAP has been acknowledged as a key component for engineering bone tissue constructs [24, 25]. Biomimetic mineralization is a powerful approach for the fabrication of organic/nano-HAP composite materials with complex shapes and hierarchical organization. In an open pore scaffolds, nano-HAP would enable tissue penetration by attracting the cells toward it, resulting in better biointegration [26], as well as mechanical/dimensional integrity of the scaffold.

Above all, our work aims to fabricate asymmetric polysaccharide composite membrance with two different surfaces. Positive CS and negative HA are composited by electrostatic interaction and reinforced by a certain ratio of KGM, which forms one smooth and dense outer surface to inhibit the ingrowth of cells from gingiva. The other porous and coarse part was fabricated by gel freeze-drying and mineralization to improve the growth of the bone tissue. Details of the study are reported herein.

2. MATERIALS AND METHODS

2.1. Materials

CS with a molecular weight of 1×10^5 and deacetylation degree of 85% was obtained from Sigma-Aldrich Co. (USA). KGM was purchased from Tianyuan konjac Co. (Hubei,China). HA was bought from Furida Biotech. (Jinan, China), and was purified before use. High glucose Dulbecco's Modified Eagle's Medium (DMEM) and fetal calf serum were obtained from Hyclone Inc. (USA). 0.25% trypsin-EDTA was obtained from GIBCO Inc. (USA). Phalloidia-TRITC and DAPI was ordered from Sigma-Aldrich Co. (USA). AKP kit was bought from Jian cheng. (Nanjing, China). M-3T3 cell (mouse fibroblast) and MC3T3-E1 was supplied by Guangzhou Red-Cross Hospital (China). All other chemicals and reagents used were analytical grade.

2.2. Solution Casting to Prepare the Smooth Composite CS/KGM/HA Membranes

HA powders were dissolved in distilled water to prepare a 0.3 wt% solution and then mixed with NaOH solution (0.1M), with volume ratio of 4: 1, to obtain an alkaline HA solution. 1 wt% CS solution (in 1 wt% acetic acid solution) was mixed with 1 wt% KGM aqueous solution, and the weight percent of CS was predetermined as 53.3%, 56.7%, 63.3% and 66.7%, 76.7% respectively. The alkaline HA solution was then added into the CS/KGM solution with the ratio of 1: 4 (v/v) under magnetic stirring to get a translucent solution. The mixture was stirred constantly to obtain homogeneous emulsion for 1h. Finally, the emulsion was cast onto petri dishes and dried at 40°C until the dry smooth membranes were obtained. The composite membranes in petri dish were kept at -80°C for next procedure.

2.3. Freeze-Drying to Fabricate Porous Surface of the Composite Membranes

HAP, CS and KGM powders were dissolved in 1 wt% nitric acid, with constant stirring to obtain a uniform solution, where the concentration of the polymers was 3 wt%, the mass ratio of HAP/polymers was 1: 4 and the optimal ratio of CS/KGM was determined according to the above results. The ternary

solution was cast onto the pre-cooled CS/KGM/HA composite membranes（-80°C）, and was then fast transferred to -80°C freezer. The composites were finally freeze-dried.

2.4. Mineralization and Aging of the Composite Membranes

The mineralization of the composites was adapted from our earlier work[26]. In brief, the composite membranes were placed in wide-mouth bottles containing 0.3 g urea and 20mL mix-solvent of ethanol and distilled water (3: 1, v/v). This mixture was adjusted to pH 10 by saturated solution of sodium hydroxide. Finally, the bottles were tightly closed and kept in the oven at 60°C for 4, 8, and 12 h respectively. The products were thoroughly washed with 85% (v/v) ethanol, and freeze-dried.

2.5. Characterization of the Composite Membranes

The composition of the dense and smooth layer was analysed by Fourier Transform Infrared spectrometer (FTIR, VERTEX 70).

The tensile strength of the smooth membranes in dry and wet state was tested by Shmadzu AG-1 universal testing machine (Z005). The membranes were cut into about 20 mm ×10 mm strips. The strips were kept in distilled water to prepare the wet samples for 5 h. The test was carried out at room temperature with the extension speed of 1mmmin^{-1} (n=3).

The crystal structure was determined with a powder X-ray diffractometer (XRD, D8 X-ray diffractometer) employing the Cu–Kα line. Data was collected from 10 to 80° (2θ values), with a step size of 0.02°, and a counting time of 1 s per step. Polarizing optical microscope (POM, Axioskop 40, Carl Zeiss, Germany) was also employed for the analysis of the crystallinity of the smooth layer.

For the characterization of the porous part, XRD was utilized to determine the crystallinity with the same parameter as mentioned above. The distribution of the inorganic phase and the detailed structure of internal were observed by transmission electron microscopy (TEM, Philips TECAI-10). To prepare the TEM samples, the composites were ground and dissolved in dilute acetic acid (0.1 wt %), followed by washing and drying. A scanning electron microscope (SEM, JSM26390LV) was utilized to investigate the surface topography and microstructure of the asymmetric membranes, with scanning voltage 20.0 kV.

2.6. Cell Seeding and Culture

All the test samples were sterilized by Co^{60} (5 kgy) and further rinsed three times with phosphate buffered saline (PBS), following by exchanging with cell culture media for overnight.

The inhibition efficiency to fibroblast was investigated on the smooth side of CS/KGM/HA composite membranes (without porous side). M-3T3 fibroblasts were used for cell culture experiments *in vitro* [23]. P3 fibroblasts in complete medium with concentration of 5.26×10^5 cells/mL were dropped onto the test samples placed in culture petri dishes (100 mm) with high-glucose DMEM medium supplemented with 10% (v/v) fetal bovine serum (FBS). Cell culture was maintained in an incubator equilibrated with 5% CO2 at 37°C. After incubation for 5 h, all the samples were transferred to new plates and supplied with 3mL complete medium; media was changed every two days during this experiment. Cell morphology was observed with a phase inverted microscope and cell adhesion and proliferation were evaluated as well

Preosteoblast MC3T3-E1 in about 5×10^5 cells/mL was seeded onto the porous CS/KGM/HA/HAP part of the asymmetric membranes (Ø10 mm×8 mm) with similar procession [27]. The thin samples with thickness of c.a.1 mm were taken for confocal laser scanning microscopy investigation (CLSM, TLS SP2, Leica,). Cells were incubated for a predetermined time to investigate cell morphology, cell adhesion, cell viability and AKP activity respectively.

2.7. Morphology of Adherent Preosteoblast

MC3T3-E1 was seeded on samples and inubated for 5 says. After incubation, the culture medium was removed and rinsed with PBS for three times. Thereafter, the adherent cells were fixed with 4% paraformaldehyde for 30 min, followed by rinsing rinsed twice with PBS.

CLSM observation of the action cytoskeletons: The thin samples were treated with 1% (v/v) Triton X-100 in PBS to permeabilize the cells for 5 min. After rinsing twice with PBS, the nonspecific binding sites were blocked by incubation with 1% (w/v) BSA for 20 min. The actin cytoskeletons were stainied by incubation with Phalloidia-TRITC (20 μg ml^{-1}) for 30 min. After

rinsing with PBS, the cell nuclei were contrast-labeled in blue by DAPI. The samples were rinsed with PBS and then mounted on glass slides using Fluoromount.

SEM observation: The fixed membrane were dehydrated in a graded series of ethanol and dried by critical point drying. The cryofractured samples were coated with a thin gold layer by Ion diffraction instrument, and observed by SEM.

2.8. Cell Adhesion on the Course Surface

After incubation for 12 h, MC3T3-E1 in the old medium and those that adhered to each well of the old tiss-culture plates were collected and counted by a hemocytometer, regarded as the number of unattached cells (Nu). The difference between the number of seeded cells and the number of unattached cells was considered as the number of attached cells held by the materials. The cell seeding efficiency of each sample was calculated by dividing the number of adhered cells by the number of seeded cells according to the following equation (n =3).

Percent cell adherence ratio (%)

= [(Ns-Nu)/Ns] ×100%.

Where Ns is the number of seeded cells and Nu is the number of unattached cells.

2.9. Cell Viability on the Coarse Surface

The protocol was adapted from literature methods. Briefly, DMEM supplemented with 80 µl of MTT (3-(4,5-Dimethylthiazol-2-yl)-2,5-diphenyltetrazolium bromide) reagent (c = 0.5 g/l) was added to each well and incubated at 37°C for 4h. Before measuring, MTT solution was carefully aspirated.Then, 600 µl of DMSO was added to each well, and the sampls were again incubated in a shaker at 37°C for another 5 min to dissolve the formazan crystals. Absorbance readings of DMSO extracts were performed at 492 nm with reference of 690 nm measured by Multiskan Mk3 microplate reader (Thermo). Cell viability was calculated by dividing the number of viable cells by the number of total cell number determined experimentally.

2.10. The Determination of the AKP Activity

The differentiation performance of MC3T3-E1 was analyzed by alkaline phosphatase (AKP) enzyme activity after culturing for 7, 14 and 21 days. The cell/membrane constructs were broken into small pieces, rinsed with PBS and dried in air for 10min. Then, those pieces were lysed with 0.1% (v/v) Triton X-100 for 30 min. The collected lysates were centrifuged at 13,000 rpm at 4°C for 5 min. The AKP activity of the supernatant was detected by the AKP kitand the mixture was incubated at 37°C. Absorbance of these samples was measured at 405 nm under normal condition.

using an ultraviolet–visible spectrophotometer.

2.11. Statically Analysis

All results are represented as mean ± SD. Data were analyzed with SPSS® v16.0 (SPSS, Chicago) software, using a Statistical Product and Service Solutions (SPSS). Values of $p \leq 0.05$ were considered to be statistically significant, and is indicated by asterisks in the figures.

3. RESULTS AND DISCUSSION

3.1. Characterization of the Smooth Layer

CS and KGM are with similar molecular structure and both possess positive charges, therefore the blending of these two solution was easily to be controlled. However HA is a linear negative polymer, which tends to aggregate once encountering with CS or KGM. The useful but very simple technique to fabricate the uniform ternary composite in this work is to prepare an alkaline HA solution, which helps to create alkaline microenvironment as the three components meeting, to impede the protonation of $-NH_2$ in CS and KGM and therefore to decrease the amounts of positive charges.

The FT-IR spectra (Figure **1**) of raw chitosan exhibited the characteristic bands at 1648 cm^{-1} (amide I), 1554 cm^{-1} (amide II) and 1411 cm^{-1} (amide III). Wave number 1026 cm^{-1} was the primary amino groups ($-NH_2$) at C_2 position of glucosamine. Stretching of primary alcoholic groups ($-CH_2OH$) was at 1056 cm^{-1}. In the infrared spectra of CS/KGM/HA composite membranes, strong absorption peaks of -OH and N-H aggregates formed at 3243 cm^{-1} peak. 2913cm^{-1} was for the asymmetric stretching vibration of $-CH_3$ and $-CH_2$. COO^- in HA is one electron conjugated system, so there will be a strong absorption in two places: near 1554 cm^{-1} for anti-symmetric contraction vibration and near 1400 cm^{-1} COO^- for symmetric contraction vibration, which were overlapped with the amide of CS, so the two peaks got stronger.

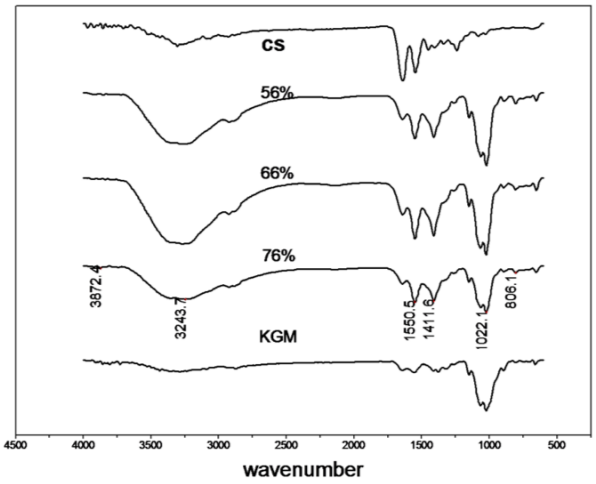

Figure1: FT-IR spectra of the composite membrane materials.

The tensile strength of the composites was influenced by CS content in both dry and wet condition, as shown in Figure **2**. The dry composite membranes with CS content of 56.7% possess the highest tensile strength, (43 Mpa), much higher than the pure CS ones (30 Mpa). The tensile strengths of the wet membranes decreased dramatically, and the highest average value was only 3.13 MPa for the membranes with CS content of 56.7%. With the increase of CS content, *i.e*. with decrease of KGM content, the strength decreased to about 1.5 MPa. Furthermore the results show that the addition of the KGM increased the elongation ratio as well. The average elongation for the membranes with 56.7% CS content was 161, much higher than the pure CS membranes (77). Accordingly, the CS content of 56.7% was selected for the further study.

Figure **3** shows the crystallinity of the membranes. The composite membrane possess a glucomannan characteristic diffraction peaks at around 20°, and the characteristic peaks of chitosan at about 25 °(Figure **a**). However, the bump or wide peak revealed that the crystallinity of the composite membranes was very low.

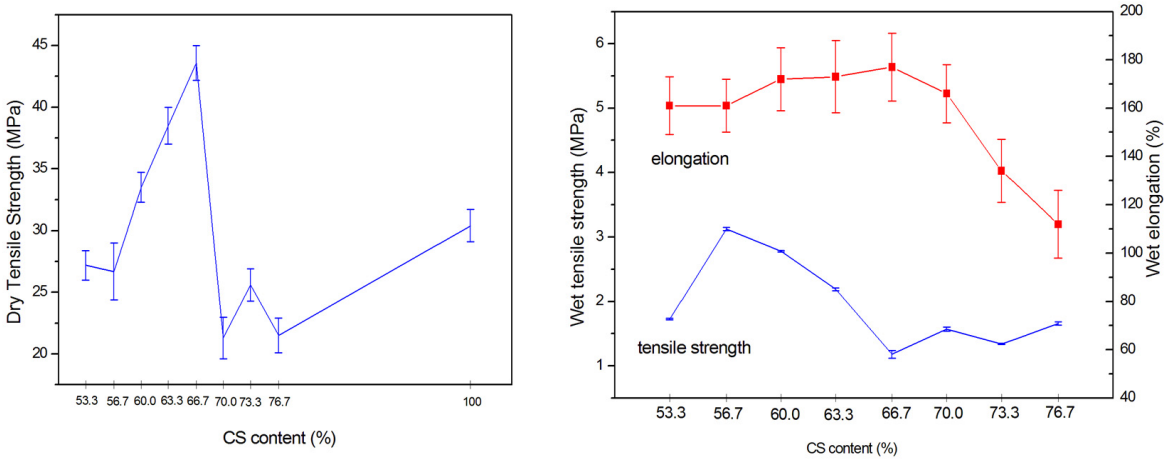

Figure 2: Effects of the CS content on tensile strength in dry (**a**) and wet state (**b**).

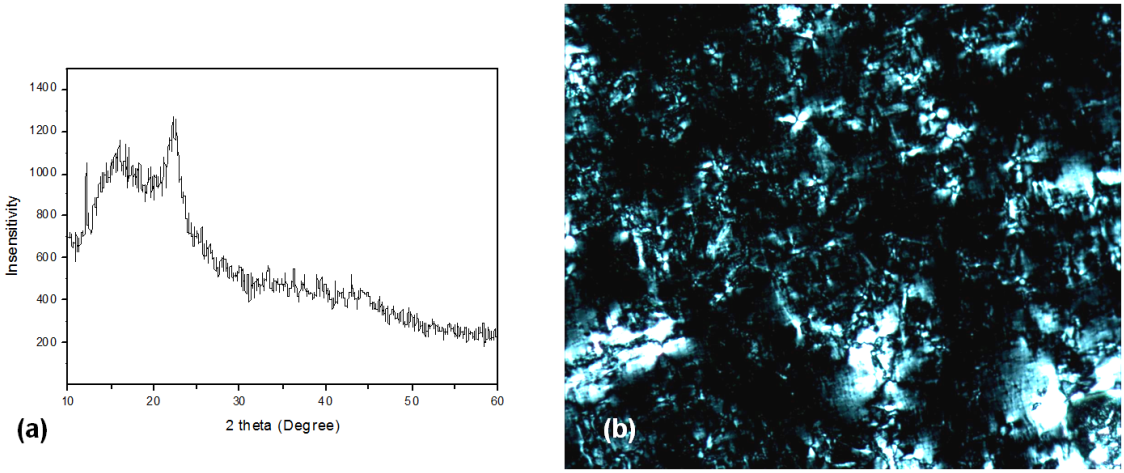

Figure3: Crystallinity of the composite membranes (CS-56.7%): (**a**) XRD pattern, (**b**) POM image.

In the POM image, small amount of spherulit were visible on the membrane surface, which further demonstrate the weak crystallinity of the membranes.

3.2. The Structure of the GBR Membranes

The asymmetric membranes were fabricated in two steps. The smooth and dense layer was prepared priorily, followed by casting of the polysaccharide mixed solution at low temperature. The contacting surface of the dense layer will undergo swelling immediately after the casting, due to dissolution by the acid solution in short time, and the molecules near the interface of the two parts would interpenetrate. The penetration and the similarity of the two phases would create a firm bonding at the interface. Therefore, though the asymmetric membranes were prepared in two steps, two parts will be integrated.

Figure **4** shows the XRD patterns of the mineralized porous surface of the asymmetric GTR membranes and the raw HAP powders. The Bragg peaks observed approximately at 26, 28, 29, 30-35, 39, 46, 49, and 50º (2θ) are corresponding to the pure phase HAP [24].Samples without aging showed a variety of calcium salt composition according to the PDF card, and the main CaP salts were $Ca_4(PO_4)_2O$ (TTCP) and $CaHPO_4$ (DCPD). With prolonged aging time, TTCP and DCPD disappeared and HAP formed. However, the three main base diffraction peaks (approximately 32°) of the samples corresponding to the HA (211), (112), (300) crystal plane, demonstrated obvious widening and diffusion phenomenon, which indicated a smaller crystalline size and lower crystallinity. The intensity ratio of the peak of 26° to 32° increased significantly with increasing aging time, suggesting that the aging procedure was benefit for the growth of the crystalline along the (002) crystal plane, *i.e*. preferentially along the c-axis direction (Figure **4 b-d**).

The complexation ability of $–NH_2$ in CS with Ca^{2+} is strong and it gets the most at pH 9-11[28]. In alkaline solution, during the co-precipitation stage, CaP salts grow spatially periodically at the active site of the $–NH_2$, which also leads to the even distribution of the CaP in the polymers substrate. Calcium phosphate such as TTCP and DCPD formed at the early stage of the reaction, which can be regarded as transition phase or precursor, since HAP phase is more stable than other salts stated above in alkaline aqueous. At 80℃, urea decomposed into CO_2 and NH_3, then dissolved in aqueous solution and hydrolyzed to HCO_3^- or CO_3^{2-} and NH_4^+ in solution. These ions kept the solution weak alkaline for the slow hydrolysis of calcium phosphate and the crystallization of HAP [29]. Moreover, distance between adjacent Ca （d_{Ca}=0.344×3=1.03nm）in HAP crystal structure is equal to the c-axis parameter (1.03nm) of CS molecule[30], which determined the growth of crystalline HAP during the aging procedure preferred to the orientation of the c-axis.

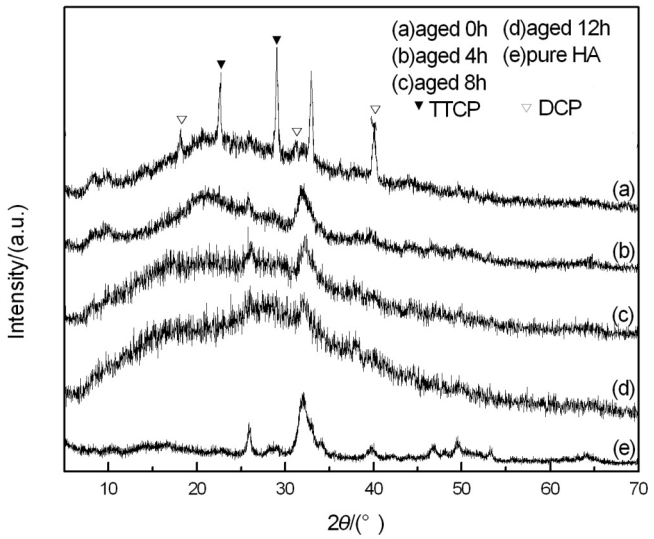

Figure 4: XRD patterns of the porous composite surface prepared with different aging time at pH=10.

For the following study, aging time for 8h was selected.

TEM observation of the composites with aging-8 h treatment were shown in Figure **5**. These tape or flake-like particles exhibit a relatively uniform appearance and good dispersibility. HAPs have an average size of about 20 nm × 200 nm, with structure and size are similar to that of HAP in bone (diameter of 15-30nm, 200-400nm in length). The TEM diffraction pattern in Figure **6** (**c**) was taken from the HAP flake and clearly shows that the crystallinity was low.

The morphology of the asymmetric membranes was shown in Figure **6**. The smooth surface of the membranes (Figure **6 a-b**) showed no obvious pores, which will be benefit for preventing the cells invasion from surrounding soft tissues. This dense top layer was formed by conventional solution casting, *i.e*. the morphology of the membranes was dependent on the surface of the container.

On the rough side of the asymmetric membrane (Figure **6 c-f**), open macro-pores distributed evenly on the surface, and the diameter of the pores ranged from

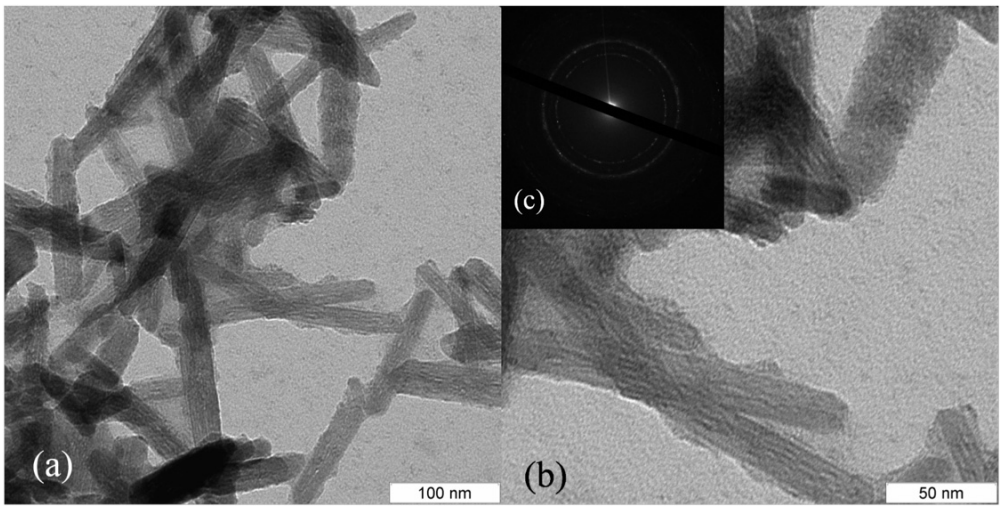

Figure 5: TEM images and diffraction pattern of the apatite aging for 8h.

10 to 100 μm. The porous surface possessed the shape of porous-sponge to enhance the permeability, water absorption, cell adhesion and proliferation, which would be benefit for osteoconduction as a GBR membrane. With larger magnification (Figure **e-f**), more details of the sponges were shown that the walls of the interconnecting pores were uniform polymers/apatite composites without evident phase separation. The results were much different from that of the earlier study[26], which were rod-like nanometer crystals settling on the chitosan matrix and inner pores. The main reason is that in this mineralization procedure HAP powders were used directly as the source of Ca and P with accurate ratio of 1.67, which were pre-dissolved uniformly in the polysaccharide polymers solution. Therefore, the mineralization was bottom-up and the combination of the apatite/polymers was on atomic levels.

3.3. The Cell Proliferation of the Asymmetric Membranes

The adhesion ratio of MC3T3-E1 on the asymmetric CS/KGM/HA/HAP membranes and CS/KGM/HA sponges were 85.79±2.38 and 79.33±4.08, respectively (Table **1**). Both the samples showed high cell seeding efficiency. The higher adhesion ratio on asymmetric membranes may be due to the mechanical properties and topological surface brought by HAP as well as the porous structure, which was benefit for cell adhesion and spreading to a certain extent.

A comparison of the proliferation of fibroblasts on the petri-dish and CS/KGM/HA membranes were made after seeding for 5 days, as presented in Figure **7** (**a**) and (**b**). The morphology of the cells on the petri dish was spreaded to fusiformis with larger numbers. In note contrast, the number of the cells decreased and the morphology was in less extension on the composite membrane. The reasons of the inhibitation of growth of fibroblast can be explained with the composition and structure of the smooth surface of the asymmetric membranes: the highly-hydrophilic HA possess inherently inhabitation to fibroblast [31, 32] and the dense surface exhibits protein resistant properties because of its tendency to bind strongly with water molecules, resulting in the formation of a hydration barrier.

Morphology and ECM distribution of MC3T3-E1 after 5 days growth on the porous membranes were observed by CLSM and SEM respectively, as shown in Figure **7** (**c-d**), Cells were homogeneously distributed in the composite sponges and almost fully covered in

Table 1: Adherence Ratio of ME-3T3 on the Asymmetric Membranes and Pure CS Scaffolds

Samples	Seeded Cells ($\times 10^4$)	Unattached Cells ($\times 10^4$)	Cell Adhesion Rate (%)
CS/KGM/HA/HAP	10.06	1.43±0.24	85.79±2.38
CS/KGM/HA	10.06	2.08±0.41	79.33±4.08

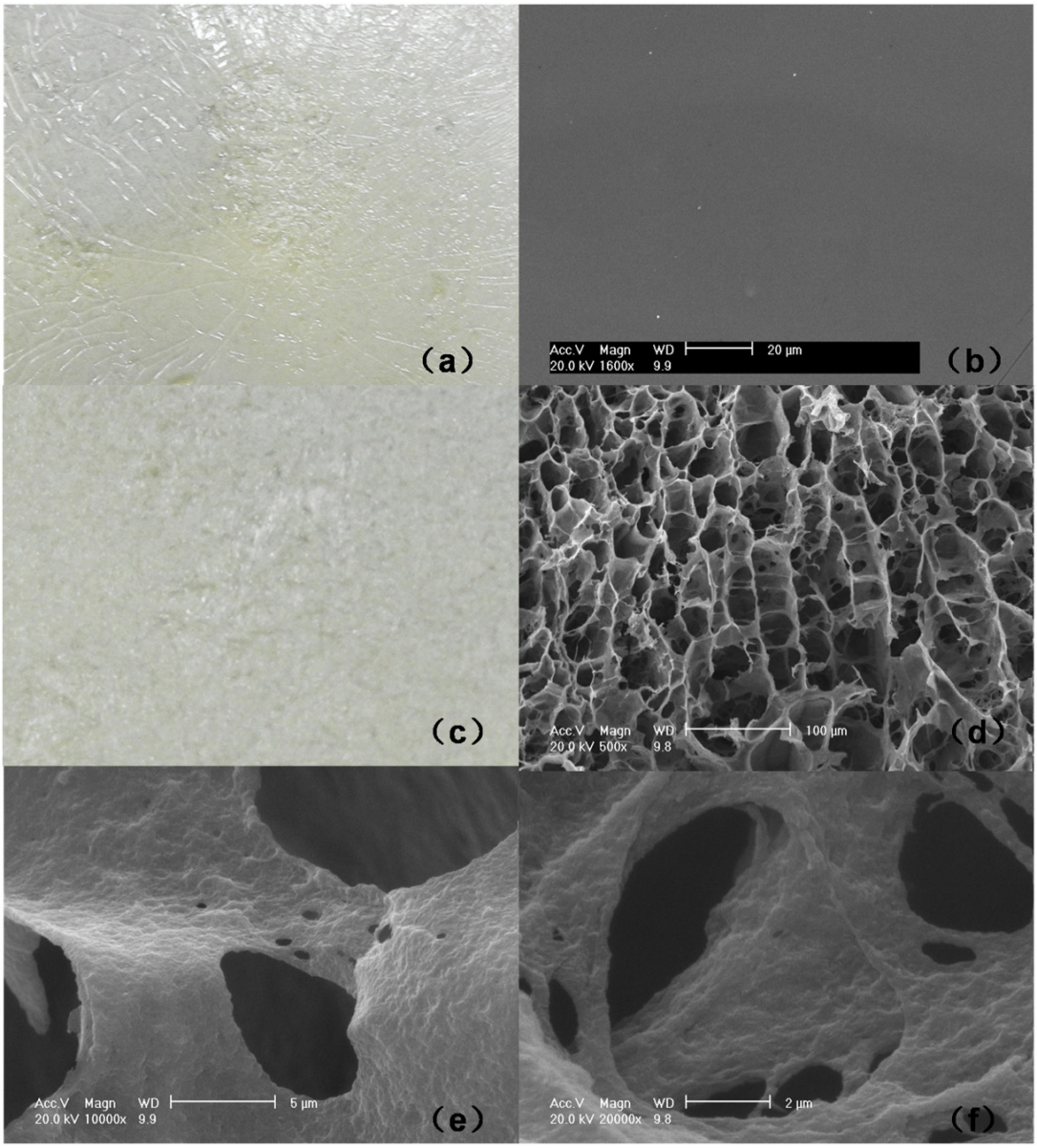

Figure 6: Morphology of the smooth surface (**a, b**) and porous surface (**c-f**) of the asymmetric membranes (aging for 8h). Figure (**a**) and (**c**) are photos taken by Nikon digital camera. Figure (**b**) and (**d**)-(**f**) are SEM images.

the pores and penetrated into the wall of the pores. Furthermore, pronounced cell layers were observed while the cells illustrated good adhesion condition and tended to growing and migration towards the holes. This is mainly because the better biocompatibility of the material and the special porous structures. In a word, the morphology of the cells was full and each cell was attached by the secreted ECM surrounding the cells.

3.4. Cell viability on the coarse surface

Figure **8** shows the results of the MTT assay. The relative activity of the cells on the sponges for 1 d was around 60-70%, comparing to the control group (Figure **8a**). It was assumed that a certain amount of cells in the pores might not well adhered, and the wet sponges shall dilute the MTT concentration which lead to incomplete reaction. With the prolonged culture time, the cell activity of the CS/KGM/HA group does not increase or decrease obviously, but the values for the CS/KGM/HA/HAP improved dramatically, and the statistical difference with the control group was significantly reduced. According to the relative viability curve in Figure **8b**, cells in the CS/KGM/HA/HAP grew slowly from day 1 to day 5, but rapidly onwards, which was close to the control group at D7. The proliferation ratio of cells seeded on the CS/KGM/HA/HAP was greater than on the CS/KGM/HA and control group,

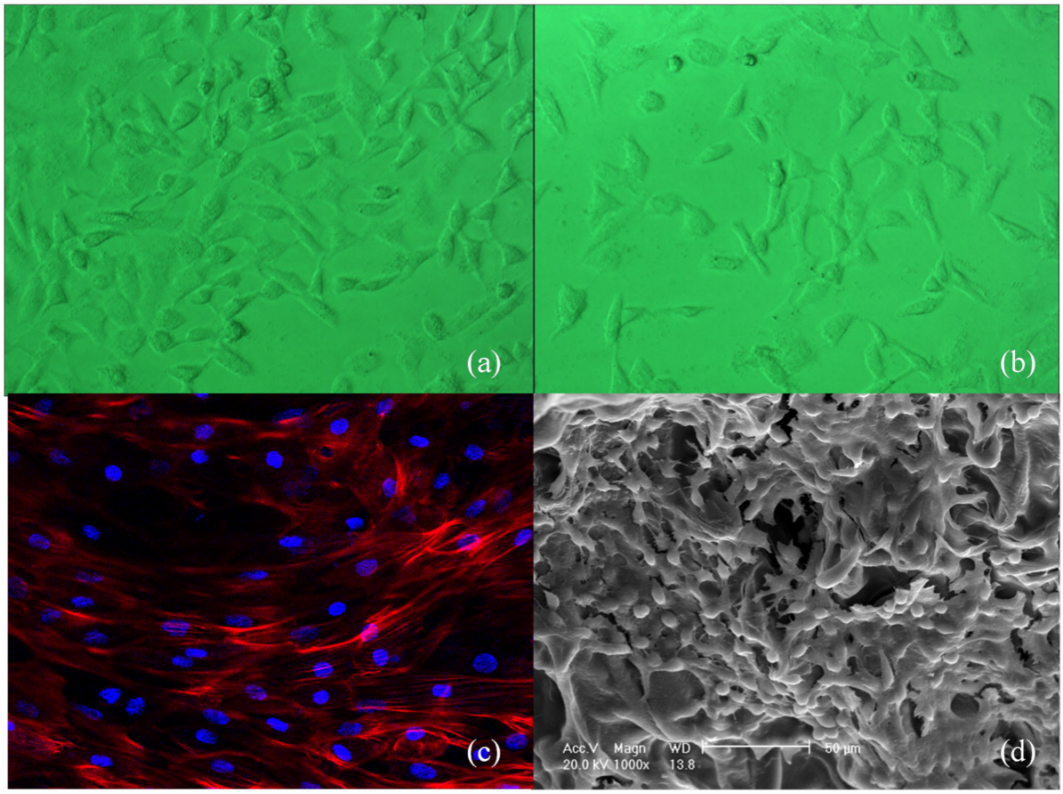

Figure 7: Cells on the membranes after 5d cell culture. Phase inverted microscope images of fibroblast on petri dish (**a**) and on the CS/KGM/HA smooth surface (**b**) (×100); CLSM image (×100) and SEM image of the MC3T3-E1 on the CS/KGM/HA/HAP porous surface (**c-d**).

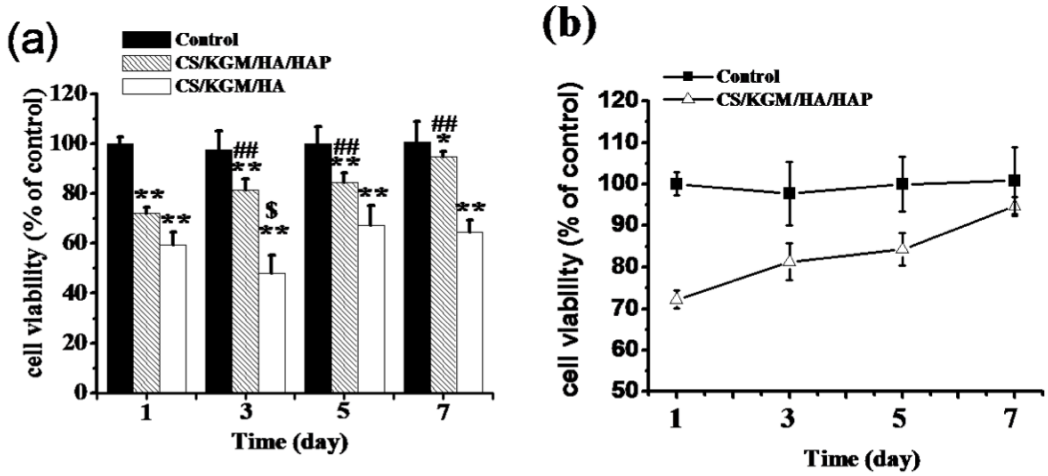

Figure 8: Relative cell viability of the cells on the sponges by MTT assay. Values comparison between sponges and the control: *P<0.05 ; **P<0.01. Values (for CS/KGM/HA/HAP) comparison of D3, D5 and D7 with D1: $^{\#}$P<0.05 ; $^{\#\#}$P<0.01. Values (for CS/KGM/HA) comparison of D3, D5 and D7 with D1: $^{\$}$P<0.05.

indicating that HAP plays a significant role on the promotion of cell growth.

3.5. AKP Activity of the MC3T3-E1

AKP activity was used as a biochemical marker for determining the differentiation of the pre-osteoblast phenotype to the mature osteoblast phenotype. Figure **9** demonstrates that AKP expression was low at day 7, and the values for group B and C were 42.16±1.47 and 32.34±1.45 respectively, which were higher than that of the control group. Significantly high AKP activity of cells was found with increasing the incubation time, and accompanied by more pronounced differences among the three groups. The values for the CS/KGM/HA/HAP group increased rapidly with elongated culturing time

especially at day 21, showing the highest AKP expression, suggesting the coefficients of the polysaccharide composites and HAP to improve the expression of AKP. An ideal scaffold such as HAP for bone regeneration should promote early mineralization and support new bone formation[33, 34], therefore calcium phosphate bioceramics such as HAP and its composites HAP/COL can induce more rapid osteoblast differentiation and mineralization [35].

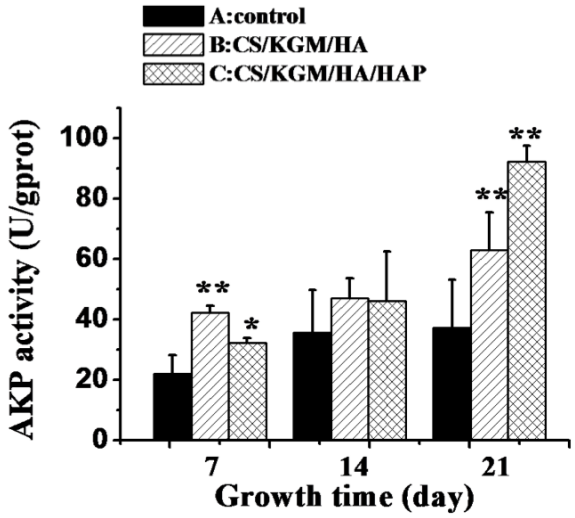

Figure 9: The AKP activity of the cells on the membrane after 7 , 14 , 21days. Comparison of CS/KGM/HA and CS/KGM/HA/HAP with the control group: *P<0.05, **P<0.01.

4. CONCLUSIONS

In this study, deeply mineralized polysaccharide composite membranes with asymmetric structures have been successfully prepared with CS, KGM and HA by two-step process. The dense and smooth surface of the membrane effectively prevented the invasion of fibroblasts , while the porous mineralized part provided enough space for the ingrowth of bone cells. Therefore, the composite membranes will be ideal candidate for regeneration of periodontal regeneration.

ACKNOWLEDGEMENTS

The work was supported by National Natural Science Foundation of China（31270021 and 81171459）and Research fund for the excellent doctorial dissertation of Guangdong Province (sybzzxm201121).

REFERENCES

[1] Keles GC, Sumer M, Cetinkaya BO, Tutkun F, Simsek SB. Effect of autogenous cortical bone grafting in conjunction with guided tissue regeneration in the treatment of intraosseous periodontal defects. Eur J Dent. 2010; 4: 403-11.

[2] Stavropoulos A, Wikesjö UM. Influence of defect dimensions on periodontal wound healing/regeneration in intrabony defects following implantation of a bovine bone biomaterial and provisions for guided tissue regeneration: an experimental study in the dog. Journal of clinical periodontology. 2010; 37: 534-43. http://dx.doi.org/10.1111/j.1600-051X.2010.01566.x

[3] Bottino MC, Thomas V, Schmidt G, Vohra YK, Chu T-MG, Kowolik MJ, *et al*. Recent advances in the development of GTR/GBR membranes for periodontal regeneration—a materials perspective. Dental Materials. 2012; 28: 703-21. http://dx.doi.org/10.1016/j.dental.2012.04.022

[4] Singh VP, Nayak DG, Uppoor AS, Shah D. Clinical and radiographic evaluation of Nano-crystalline hydroxyapatite bone graft (Sybograf®) in combination with bioresorbable collagen membrane (Periocol®) in periodontal intrabony defects. Dental research journal. 2012; 9: 60. http://dx.doi.org/10.4103/1735-3327.92945

[5] Patel S, Kubavat A, Ruparelia B, Agarwal A, Panda A. Comparative Evaluation of Guided Tissue Regeneration withuse of Collagen-based Barrier Freeze-Dried Dura MaterAllograft for Mandibular Class 2 Furcation Defects (A Comparative Controlled Clinical Study). The Journal ofContemporary Dental Practice. 2012; 13: 11-5. http://dx.doi.org/10.5005/jp-journals-10024-1088

[6] [6] Singh H, Singh H. Bioactive amnion as a guided tissue regeneration (GTR) membrane for treatment of isolated gingival recession. A case report. Indian Journal of Dentistry. 2013. http://dx.doi.org/10.1016/j.ijd.2012.12.007

[7] Yang F, Both SK, Yang X, Walboomers XF, Jansen JA. Development of an electrospun nano-apatite/PCL composite membrane for GTR/GBR application. Acta Biomaterialia. 2009; 5: 3295-304. http://dx.doi.org/10.1016/j.actbio.2009.05.023

[8] Bottino MC, Thomas V, Janowski GM. A novel spatially designed and functionally graded electrospun membrane for periodontal regeneration. Acta Biomaterialia. 2011; 7: 216-24. http://dx.doi.org/10.1016/j.actbio.2010.08.019

[9] Vaquette C, Fan W, Xiao Y, Hamlet S, Hutmacher DW, Ivanovski S. A biphasic scaffold design combined with cell sheet technology for simultaneous regeneration of alveolar bone/periodontal ligament complex. Biomaterials. 2012. http://dx.doi.org/10.1016/j.biomaterials.2012.04.038

[10] Jia J, Liu G, Yu J, Duan Y. Preparation and characterization of soluble eggshell membrane protein/PLGA electrospun nanofibers for guided tissue regeneration membrane. Journal of Nanomaterials. 2012; 2012: 25. http://dx.doi.org/10.1155/2012/282736

[11] Chhabra V, Gill AS, Sikri P, Bhaskar N. Evaluation of the relative efficacy of copolymerized polylactic-polyglycolic acids alone and in conjunction with polyglactin 910 membrane in the treatment of human periodontal infrabony defects: A clinical and radiological study. Indian Journal of Dental Research. 2011; 22. http://dx.doi.org/10.4103/0970-9290.80003

[12] Bunyaratavej P, Wang H-L. Collagen membranes: a review. Journal of periodontology. 2001; 72: 215-29. http://dx.doi.org/10.1902/jop.2001.72.2.215

[13] Mota J, Yu N, Caridade SG, Luz G, Gomes ME, Reis RL, *et al*. Chitosan/Bioactive Glass Nanoparticles Composite Membranes for Periodontal Regeneration. Acta Biomaterialia. 2012. http://dx.doi.org/10.1016/j.actbio.2012.06.040

[14] Xu C, Lei C, Meng L, Wang C, Song Y. Chitosan as a barrier membrane material in periodontal tissue regeneration. Journal of Biomedical Materials Research Part B: Applied

Biomaterials. 2012; 100: 1435-43.
http://dx.doi.org/10.1002/jbm.b.32662

[15] Zhang K, Zhao M, Cai L, Wang Z-k, Sun Y-f. Preparation of chitosan/hydroxyapatite guided membrane used for periodontal tissue regeneration. Chinese Journal of Polymer Science. 2010; 28: 555-61.
http://dx.doi.org/10.1007/s10118-010-9087-9

[16] Fazio V, Cohen Z, Fleshman J, van Goor H, Bauer J, Wolff B, *et al*. Reduction in Adhesive Small-Bowel Obstruction by Seprafilm< sup> ®< /sup> Adhesion Barrier After Intestinal Resection. Diseases of the Colon & Rectum. 2006; 49: 1-11.
http://dx.doi.org/10.1007/s10350-005-0268-5

[17] Lawson KJ, Malycky JL, Berry JL, Steffee AD. Lamina Repair and Replacement to Control Laminectomy Membrane Formation in Dogs. Spine. 1991; 16: S222-S6.
http://dx.doi.org/10.1097/00007632-199106001-00009

[18] Aysan E, Bektas H, Ersoz F, Sari S, Huq G. Effects of contractubex on the prevention of postoperative peritoneal adhesion. Journal of Surgical Research. 2010; 164: 193-7.
http://dx.doi.org/10.1016/j.jss.2010.05.045

[19] Li G, Qi L, Li A, Ding R, Zong M. Study on the kinetics for enzymatic degradation of a natural polysaccharide, konjac glucomannan. Macromolecular Symposia: Wiley Online Library; 2004. p. 165-78.

[20] Liu J, Zhang L, Hu W, Tian R, Teng Y, Wang C. Preparation of konjac glucomannan-based pulsatile capsule for colonic drug delivery system and its evaluation *in vitro* and *in vivo*. Carbohydrate Polymers. 2012; 87: 377-82.
http://dx.doi.org/10.1016/j.carbpol.2011.07.062

[21] Wu D, Wen JH, Li LH, Zhao YW, Li B, Zhou CR. Preparation and Characterization of Alveolar Bone and Periodontal Ligament Interface Scaffolds. Advanced Materials Research. 2013; 647: 133-8.
http://dx.doi.org/10.4028/www.scientific.net/AMR.647.133

[22] Wikesjö UM, Susin C, Lee J, Dickinson DP, Polimeni G. Periodontal regeneration: experimental observations—clinical consequences. Endodontic Topics. 2013; 26: 4-17.
http://dx.doi.org/10.1111/etp.12022

[23] Ho M-H, Hsieh C-C, Hsiao S-W, Van Hong Thien D. Fabrication of asymmetric chitosan GTR membranes for the treatment of periodontal disease. Carbohydrate Polymers. 2010; 79: 955-63.
http://dx.doi.org/10.1016/j.carbpol.2009.10.031

[24] Danilchenko S, Koropov A, Protsenko IY, Sulkio-Cleff B, Sukhodub L. Thermal behavior of biogenic apatite crystals in bone: An X-ray diffraction study. Crystal Research and Technology. 2006; 41: 268-75.
http://dx.doi.org/10.1002/crat.200510572

[25] Daei-farshbaf N, Ardeshirylajimi A, Seyedjafari E, Piryaei A, Fathabady FF, Hedayati M, *et al*. Bioceramic-collagen scaffolds loaded with human adipose-tissue derived stem cells for bone tissue engineering. Molecular biology reports. 2014; 41: 741-9.
http://dx.doi.org/10.1007/s11033-013-2913-8

[26] Li L, Li B, Zhao M, Ding S, Zhou C. Single-step mineralization of woodpile chitosan scaffolds with improved cell compatibility. Journal of Biomedical Materials Research Part B: Applied Biomaterials. 2011; 98: 230-7.
http://dx.doi.org/10.1002/jbm.b.31811

[27] Zhao M, Li L, Li X, Zhou C, Li B. Three-dimensional honeycomb-patterned chitosan/poly(L-lactic acid) scaffolds with improved mechanical and cell compatibility. Journal of Biomedical Materials Research Part A. 2011; 98A: 434-41.
http://dx.doi.org/10.1002/jbm.a.33132

[28] Li H, Zhu M-y, Li L-h, ZHOU C-r. Preparation of in situ-deposited hydrxyoapatite on chitosan scaffold. Journal of Functional Materials. 2006; 37: 909.

[29] T FULMER M, Brown P. Hydrolysis of dicalcium phosphate dihydrate to hydroxyapatite. Journal of Materials Science: Materials in Medicine. 1998; 9: 197-202.
http://dx.doi.org/10.1023/A:1008832006277

[30] Okuyama K, Noguchi K, Kanenari M, Egawa T, Osawa K, Ogawa K. Structural diversity of chitosan and its complexes. Carbohydrate Polymers. 2000; 41: 237-47.
http://dx.doi.org/10.1016/S0144-8617(99)00142-3

[31] Kamel RM. Prevention of postoperative peritoneal adhesions. European Journal of Obstetrics & Gynecology and Reproductive Biology. 2010; 150: 111-8.
http://dx.doi.org/10.1016/j.ejogrb.2010.02.003

[32] Pados G, Makedos A, Tarlatzis B. Adhesion Prevention Strategies in Laparoscopic Surgery. 2013.

[33] Li X, Fan Y, Watari F. Current investigations into carbon nanotubes for biomedical application. Biomedical Materials. 2010; 5: 022001.
http://dx.doi.org/10.1088/1748-6041/5/2/022001

[34] Biazar E, Heidari Keshel S, Rezaei Tavirani M, Jahandideh R. Bone formation in calvarial defects by injectable nanoparticular scaffold loaded with stem cells. Expert opinion on biological therapy. 2013; 13: 1653-62.
http://dx.doi.org/10.1517/14712598.2013.840284

[35] Lee HJ, Lee JK, Lee H, Carter JE, Chang JW, Oh W, *et al*. Human umbilical cord blood-derived mesenchymal stem cells improve neuropathology and cognitive impairment in an Alzheimer's disease mouse model through modulation of neuroinflammation. Neurobiology of aging. 2012; 33: 588-602
http://dx.doi.org/10.1016/j.neurobiolaging.2010.03.024.

Received on 15-04-2015 Accepted on 03-05-2015 Published on 06-05-2015

http://dx.doi.org/10.15379/2409-3394.2015.02.01.7